Applied Catalysis B: Environmental 179 (2015) 95–105

Contents lists available at ScienceDirect

Applied Catalysis B: Environmental

journal homepage: www.elsevier.com/locate/apcatb

Influence of the surface oxygenated groups of activated carbon on preparation of a nano Cu/AC catalyst and heterogeneous catalysis in the oxidative carbonylation of methanol

Guoqiang Zhang, Zhong Li*, Huayan Zheng, Tingjun Fu, Yubo Ju, Yuchun Wang

Key Laboratory of Coal Science and Technology of Ministry of Education and Shanxi Province, Institute of Coal Chemical Engineering, Taiyuan University of Technology, Taiyuan 030024, Shanxi, China

ARTICLE INFO

Article history:
Received 27 November 2014
Received in revised form 28 April 2015
Accepted 1 May 2015
Available online 7 May 2015

Keywords:
Cu/AC catalyst
Surface oxygenated groups
Dispersion
Valence distributions
Deactivation

ABSTRACT

Coconut shell activated carbon (AC) is treated by nitric acid and used as a support to prepare nano-copper heterogeneous catalysts for oxidative carbonylation of methanol to dimethyl carbonate. AC supports and their corresponding catalysts are characterized intensively by BET, XPS, XRD, TEM, N_2O chemisorption, CO adsorption, and TPR. The results show that the concentrations of nitric acid do not significantly changes the specific surface area and textural property of AC. But the oxygenated groups which result in acidic properties, such as lactone, carboxyl and phenol groups, are formed on AC surface during the acid treatment process and increase with the increasing concentration of nitric acid. The increased surface oxygenated groups not only influence the dispersion but also the valence distributions of copper species. When copper supported on the AC treated by 4 M HNO_3, the Cu/AC catalyst shows the optimal catalytic performance for oxidative carbonylation of methanol to dimethyl carbonate, which might be ascribed to the highest dispersion of Cu^+ and Cu^0 species. The average conversion of methanol and space-time yield of DMC (STY_{DMC}) within 10 h for the catalyst have reached 9.2% and 229 mg g^{-1} h^{-1}, respectively. The deactivation of Cu/AC catalysts is attributed to the agglomeration of copper species. Besides, the STY_{DMC} of per $S(Cu^+ + Cu^0)$ for the acid treated Cu/AC catalysts is very similar and less than that of the original Cu/AC catalyst which may be induced by the AC surface oxygenated groups itself but not the ratio of Cu^+/Cu^0.

1. Introduction

Supported Cu-based catalysts have been widely investigated in hydrogenation reaction (such as hydrogenation of CO to methanol and ethanol [1,2], dimethyl oxalate to glycol [3]), hydrogenolysis reaction (such as hydrogenolysis of glycerol to 1,2-propanediol [4,5]), oxidation reaction (such as oxidation of SO_2 to SO_3 [6], CO to CO_2 [7]), reduction reaction (such as reduction of nitric oxide to N_2 [8], nitrate to N_2 [9]) and oxidative carbonylation reaction (such as methanol to dimethyl carbonate and ethanol to diethyl carbonate [10,11]). Many materials including AC, Al_2O_3, CeO_2, ZrO_2, SiO_2 and zeolite [8,12–19] are employed as supports to provide a large surface area for copper species dispersion. Among the above mentioned catalyst supports, AC exhibits the favorable physical and chemical characteristics for the preparation of a catalyst with the fine dispersion of an active copper species on the AC support [19–21]. This fact has drawn researchers' attention and considerable efforts have been made to investigate the performances and characteristics of these supported Cu/AC catalysts.

It is known that the catalytic activity of supported catalyst is strongly dependent on the dispersion of active species over the support [22]. In order to obtain the fine dispersion of copper species over AC support, various techniques such as impregnation technique [7], liquid phase reduction [23], and chemical precipitation [24] have been used to fabricate Cu/AC catalyst. For example, Lu et al. [25] found the size of Cu particles was about 100–150 nm of the Cu/AC catalysts prepared by polyol reduction. Wang et al. [24] employed chemical precipitation to prepare Cu/AC catalysts and showed the crystalline size of Cu was about 42.6 nm. Besides, previous studies have shown that the surface oxygenated groups enhance the hydrophilicity of the AC allowing easy access of metal salt solutions during the impregnation process and provide additional nucleation sites, which could further improve the dispersion

* Corresponding author at: No. 79 Yingze West street, Taiyuan 030024, China. Tel.: +86 351 6018526; fax: +86 351 6018526.
E-mail address: lizhong@tyut.edu.cn (Z. Li).

http://dx.doi.org/10.1016/j.apcatb.2015.05.001
0926-3373/

of active species [26,27]. Generally, AC pretreatment by HNO_3 is believed to be an available way for the formation of more surface oxygenated groups onto AC [23]. Zhu et al. [28] reported that AC treated by HNO_3 had more active surface complexes such as carboxyls and lactones, and the grain size of the supported Cu_2O decreased from 16.5 nm to 12.4 nm which led to the improved catalyst dispersion as well as the catalytic activity for the reduction of N_2O and NO. Rau et al. [29] also found that HNO_3 treatment produced more active surface complexes which improved the dispersion of CuO over AC support, and the removal efficiency of SO_2 increased from 56.4% to 84.2%. Be that as it may, the influence of the amount of surface oxygenated groups on the copper species dispersion has not been thoroughly researched so far.

In addition, the valence of copper species over the AC support also plays an important role in catalytic performance. According to previous studies [30], the high catalytic activity of Cu/AC catalyst for NO reduction in the presence of oxygen was owing to existence of CuO and Cu_2O species. But when NO reduction was conducted in the presence of NH_3, Cu_2O and metallic Cu was detrimental for the improvement of catalytic performance of CuO/AC catalysts [31]. In the synthesis of DMC by oxidative carbonylation of methanol, all the AC supported copper catalysts (Cu^0/AC, Cu_2O/AC and CuO/AC) were reported to show good catalytic activity [18,32]. Li et al. [32] reported that Cu_2O species was the best catalytic active center among the above copper species. While Ren et al. [18] found that the catalytic activity follows the order: Cu^0/AC > Cu_2O/AC > CuO/AC. Generally, the calcination temperature in the thermal treatment of copper precursor on AC is found to be crucial in controlling the valence distribution of copper species, and the higher the calcination temperature, the lower valence of copper species is formed on AC [24,30,33]. But the precursor of Cu/AC catalyst calcinated at high temperature would result in the aggregation of copper species and formation of larger particles [31]. So it is still a challenge to prepare Cu/AC catalysts with tunable valence distributions under the moderate temperature without the aggregation of copper species. The available way is to modify the surface chemistry of the AC support, especially the surface oxygenated groups, which affects the precursor/support interaction and thus influences the valence distributions of the copper species during the decomposition or reduction stage [23,34]. Chuang and Li et al. [21,23] found that more Cu_2O species were observed on AC when copper supported on AC treated by HNO_3 compared with that supported on original AC. Even so, the relationship between the amount of surface oxygenated groups and the valence distributions of copper species over the support has not been reported yet.

In this paper, coconut shell AC is treated by HNO_3 to modify the surface chemistry and used as a support to prepare supported Cu catalysts. The effect of acid treatment concentration on the carbon texture structure and surface chemistry has been studied. Then, the influence of the surface oxygenated groups (e.g., lactone, carboxyl and phenol) on the dispersion, valences distribution of the Cu/AC catalyst has also been investigated and the catalytic performances of Cu/AC catalysts for oxidative carbonylation of methanol to DMC are evaluated in a fixed bed reactor.

2. Experimental

2.1. Preparation of Cu/AC catalysts

A commercially available AC with a BET surface area of 1643 m^2/g is made from coconut shells (Xinsen Chemical Industry Co. Ltd.). The AC is pretreated with different concentrations of HNO_3 (from 2 M to 12 M) at 80 °C for 6 h, then wash with distilled water until pH 7, and eventually outgas in a vacuum at 100 °C overnight. The pretreated AC is denoted as AC-*x*, where *x* represents the concentration of HNO_3.

The catalysts with 11.2 wt.% Cu loadings are prepared by an incipient wetness impregnation method. An aqueous solution of Cu $(NO_3)_2$ is added to the support with stirring at room temperature for 6 h. After dried in air overnight at 100 °C, the precursors are calcined in nitrogen at 350 °C for 4 h. The catalysts are denoted as Cu/AC-*x*.

2.2. Characterization of AC and Cu/AC catalysts

The textural properties of the support and the catalysts were analyzed by N_2 adsorption–desorption isotherms obtained at −196 °C using Micromeritics ASAP 2020 apparatus. The surface area was obtained using Brunauer–Emmett–Teller (BET) model for adsorption data in a relative pressure range of 0.05–0.30. The total pore volumes were calculated from the amount of N_2 vapor adsorbed at a relative pressure of 0.99. The average pore diameter of samples was determined by assuming that all pores in the sample were parallel and cylindrical, by dividing the pore volume with the surface area.

The Boehm titration method was used to determine the contents of acidic sites on the AC support surface. One gram of the carbon sample was immersed into 0.1 M solutions of each of the following: sodium hydroxide (NaOH), sodium carbonate (Na_2CO_3), and sodium bicarbonate ($NaHCO_3$). The mixed solutions were sealed and shaken for 48 h and then filtered. A volume of 10 mL of the filtrate was pipetted into a flask and the excess base was titrated with HCl. The theoretical value of HCl solutions concentration was set as 0.1 M. Given the easy volatilization of concentrated HCl that may cause the inaccuracy during the preparation of HCl solution, the real value (0.094 M) was obtained via calibration with NaOH solutions by titration. The contents of various types of acidic sites were calculated using the assumptions that NaOH neutralizes the carboxylic, phenolic, and lactonic groups; Na_2CO_3 neutralizes the carboxylic and lactonic groups; and $NaHCO_3$ neutralizes only the carboxylic groups.

X-ray photoelectron spectroscopy (XPS) data were collected on an ESCALab220i-XL electron spectrometer (VG, UK) using 300 W AlKa radiation. The samples were compressed into a pellet of 2 mm thickness and then mounted on a sample holder by utilizing double-sided adhesive tape for XPS analysis. The sample holder was then placed into a fast entry air load-lock chamber without exposure to air and evacuated under vacuum (<10^{-6} Torr) overnight. Finally, the sample holder was transferred to the analysis chamber for XPS study. The base pressure inside the analysis chamber was usually maintained at better than 10^{-10} Torr. The binding energies were referenced to the C1s line at 284.6 eV from adventitious carbon.

X-ray diffraction (XRD) measurements were performed with a Rigaku D/Max 2500 powder diffractometer using Cu K α radiation (λ = 0.15406 nm) at 40 kV and 100 mA. The patterns were recorded in steps of 0.01° with the scanning rate at 8°/min from 5° to 85° under atmospheric pressure.

Transmission electron microscopy (TEM) photographs were taken with a JEOL JEM-2999FMII apparatus. Samples for TEM were prepared by placing a drop of a colloidal dispersion of ME-NiB in an isopropanol solvent onto a perforated copper grid, followed by naturally evaporating the solvent. The mean particle diameters were calculated by nano measurer software from TEM image analysis.

AAS was used for the elemental analyzes of actual copper loadings of the prepared catalysts by SpectrAA-220 AAS equipment. 50 mg of each catalyst was dissolved in a strong acid mixture and the volumes of each sample were completed to 50 ml by using deionized water.

Temperature-programmed reduction (TPR) experiments were performed out on Micromeritics AutoChem 2920 equipment. For

this, 25 mg of catalyst was loaded into a U-shape quartz reactor, and sample was degasified with argon (20 mL/min) at 200 °C for 2 h to remove physisorbed moisture. After cooling to room temperature, the gas was switched to 10% H_2 in argon flow (20 mL/min), and catalyst was heated to 1000 °C with a heating rate of 10 °C/min. Effluent gas was passed through a cold trap to trap moisture in effluent gas before reaching the thermal conductivity detector (TCD). The amount of H_2 consumption during reduction was monitored by a TCD.

The total specific surface area (S_{total}) and average particle size ($d_{average}$) of Cu/AC catalysts were determined by via N_2O chemisorption in the same apparatus as for TPR. The fresh Cu/AC catalysts were first reduced in the procedure described in the TPR experiment in a 10% H_2/Ar mixture until 450 °C and the reactor was purged with N_2 to 50 °C. Then N_2O was used to oxidize surface copper atoms to Cu_2O (s). The specific surface area of Cu was performed by dissociative N_2O adsorption on the surface of copper with the pulse titration method based on the following equations: $2Cu\,(s) + N_2O \rightarrow N_2 + Cu_2O\,(s)$. The evolution of N_2 were analyzed by thermal conductivity detector (TCD) to detect the consumption of N_2O (X) with 1×10^{19} atoms m^{-2}. $d_{average}$ in nanometers was calculated by assuming a spherical particle shape and using the equation: $d_{average}\,(nm) = 6000/\rho Cu S_{total}$, with $S_{total} = 2XN_A/1 \times 10^{19} \times (1 + a)/a$ (N_A is Avogadro's constant, a is the actual copper loading determined by AAS = m_{Cu}/m_{AC}) and ρ_{Cu} = copper density (8.92 g cm^{-3}). The dispersion $D = 2XM_{Cu}\,(1 + a)/a$. M_{Cu} is the relative atomic mass of copper (63.46 g/mol) [35].

The Cu^0 surface area (S_{Cu0}) of the catalysts was determined by via N_2O chemisorption in the same apparatus as above. The catalyst sample was placed into a U-shaped quartz tube and then N_2O was used to oxidize the surface Cu^0 atoms to form Cu_2O (s). The specific surface area of Cu was performed by dissociative N_2O adsorption on the surface of copper with the pulse titration method based on the following equations: $2Cu\,(s) + N_2O \rightarrow N_2 + Cu_2O\,(s)$. The evolution of N_2 were analyzed by thermal conductivity detector (TCD) to detect the consumption of N_2O (Y) with 1×10^{19} atoms m^{-2}. $S_{Cu0} = 2YN_A/1 \times 10^{19}$.

The Cu^+ surface area of the catalysts was determined via irreversible CO adsorption isotherms [3]. The isotherms were collected with the chemisorption module of a Micromeritics ASAP 2020 instrument. Samples were cooled to 27 °C, and a total adsorption isotherm was collected using 50–500 mm Hg CO. After evacuation for 30 min, the measurement was repeated to determine the reversible adsorption isotherm. The difference between the total and reversible isotherms was used to determine the irreversible isotherm. The irreversible adsorption was the asymptotic value obtained by averaging the irreversible isotherm points between 150 and 500 mm Hg CO. S_{Cu+} of the catalysts was estimated from the amount of CO irreversible adsorption consumption (M) with 1×10^{19} atoms m^{-2}, $S_{Cu+} = MN_A/1 \times 10^{19}$.

2.3. Catalytic activity test

The vapor-phase DMC synthesis by oxidative carbonylation of methanol was investigated in a continuous flow fixed bed reactor with 6 mm inner diameter and 45 cm length at atmospheric pressure. 0.8 g (about 1.5 ml) catalyst sample was packed in the tubular reactor and positioned in the middle of the reactor furnace. 3 ml/h Methanol was introduced by a constant-flux pump and vaporized in the pre-heater, then mixed well with carbon monoxide and oxygen together, and then entered into the catalyst bed to be catalyzed for oxidative carbonylation to DMC. The thermal gas products were directly analyzed by an Agilent 6890 GC equipped with HP-INNOWAX capillary column connected to a flame ionization detector (FID) and PROPACK-Q packed column, HP-PLOT/Q and HP-PLOT Molesieve/5A capillary columns connected to a thermal conductivity detector (TCD). MeOH, methyl formate (MF), dimethoxymethane (DMM), dimethyl ether (DME) and DMC were detected with the FID, whereas CO, O_2, CO_2 were detected with the TCD. Complete GC product analysis run time was 12 min.

3. Results and discussion

3.1. Textural characteristics analysis of AC supports and Cu/AC catalysts

The textual properties of the original AC, HNO_3 treated AC-x and the corresponding Cu/AC catalysts are characterized by N_2 adsorption–desorption instruments apparatus and shown in Table 1. The surface area and pore volume of the original AC are 1643 m^2/g and 0.86 cm^3/g, respectively. When the AC is treated by HNO_3 for 6 h at 80 °C, the surface areas of the AC supports are reduced slightly from 9% to 15% when the concentration of HNO_3 is raised from 2 M to 12 M. The $S_{Meso+macro}$ is in the range of 69–91 m^2/g with the increased concentration of HNO_3 from 2 M to 12 M. It has been reported in many works that the liquid phase oxidation by nitric acid might not significantly change the textural properties of activated carbon [36–38]. The slight decrease in AC surface area may be due to the abundant presence of oxygenated groups introduced on the surface of the activated carbon by the treatment with HNO_3, which possibly block the entry of N_2 inside the small pores, as reported by Rodrigues et al. [37]. After loading of Cu, the surface area of the copper catalysts is less than that of the respective supports. This is a result of the pores of AC being partly blocked by copper species [39]. From comparisons of the surface area and pore volume between the copper catalysts and its respective support, pore blockage is evident, which is shown by a decrease in both these characteristics.

3.2. Surface chemistry analysis of AC samples

The amount of surface oxygenated groups on the original AC and AC-x pretreated with different concentrations of HNO_3 measured by Boehm's method is presented in Table 2. The amount of all the groups resulted in acidic properties including carboxyl groups, lactonic groups and phenolic groups increase with the increased treatment concentration. The total acidity of AC treated by 12 M HNO_3 aqueous has reached 1.79 mmol/g, which is about 6 times as high as 0.33 mmol/g of the original AC support. Li et al. [40] also found that carboxyl groups, lactonic groups and phenolic groups increase with the increased HNO_3 concentration, which is similar to our experiment. The experimental results indicate that the amount of surface oxygenated groups and the total acidity on the AC are highly dependent upon the HNO_3 concentration used. The increase in the surface acidic oxygen groups of the acid treatment AC supports may be contributed to getting rid of inorganic compounds which leaves defects or discontinuities for chemisorbing oxygen in air at room temperature [41] or decompose some groups to produce more acidic groups [28,42]. In addition, HNO_3 as an oxidant may also oxidize some complexes to produce acidic groups.

XPS characterization is also carried out to analyze the surface oxygenated groups. Fig. 1A, B and C show the XPS spectra of C1s, O1s and N1s in the original and treated AC samples, respectively. The peaks centered at 284.6 eV, 286.1 eV, 287.4 eV, 289.3 eV and 290.4 eV of C1s deconvolution spectra can be attributed to graphitic carbon, phenolic, alcohol or ether groups, carbonyl or quinone groups, carboxyl acidic groups and π–π^* shake-up satellite peak, respectively [43,44]. The deconvolution of O1s spectra reveals the presence of three peaks corresponding to quinones and carbonyl groups, lactones, carboxylic anhydrides, phenol, and ether groups, carboxylic acid groups [44–46]. As seen in Fig. 1A and B, the area of

Table 1
Textual property of the AC supports and Cu/AC catalysts.

Samples	HNO_3 concentration(mol/L)	S_{BET}(m^2/g)	V_P(cm^3/g)	D_P(nm)	S_{Micro} (m^2/g)	$S_{Meso+macro}$ (m^2/g)	Decreased surface area percent (%)
AC supports	0	1643	0.86	2.55	1566	77	–
	2	1496	0.80	2.14	1414	82	8.9
	4	1480	0.80	2.16	1411	69	10.0
	8	1465	0.78	2.15	1384	81	10.8
	10	1451	0.79	2.17	1371	80	11.7
	12	1420	0.77	2.16	1329	91	13.6
Cu/AC catalysts	0	1338	0.71	2.13	1261	77	–
	2	1280	0.68	2.12	1218	62	4.3
	4	1226	0.66	2.13	1158	68	8.4
	8	1214	0.64	2.11	1140	74	9.3
	10	1121	0.60	2.16	1048	73	16.2
	12	1111	0.59	2.16	1041	70	17.0

S_{BET}: BET surface area; Vp: total pore volumes were obtained at $P/P_0 = 0.99$; Dp: average pore diameter calculated by BJH method; and S_{BET}: *t*-plot micropore area.

Table 2
Surface oxygenated groups of the AC samples.

AC samples	Carboxyl group(mmol/g)	Lactonic group(mmol/g)	Phenol group(mmol/g)	Total acidity(mmol/g)
AC-0	0.22	0.03	0.08	0.33
AC-2	0.37	0.12	0.25	0.74
AC-4	0.48	0.14	0.25	0.87
AC-8	0.71	0.15	0.34	1.20
AC-10	0.84	0.29	0.38	1.51
AC-12	1.05	0.32	0.41	1.78

all the peaks corresponding to surface oxygenated groups increases with the increase of treatment concentration which is in good agreement with the results determined by Boehm's method. The N1s spectrum of the original AC has three peaks, the peak centered at 398.4 eV, 399.7 eV and 401.3 eV are corresponding to the pyridinic N (N-6), pyrrole nitrogen (pyrrolic-N) and quaternary nitrogens (N–Q), respectively [47]. These peaks disappear in the N1s spectrum of AC-x, and new peak appeared at 405.6 eV is defined as NO_X groups [48]. Table 3 lists the carbon, oxygen and nitrogen contents of the original AC and AC-x obtained by XPS. The content

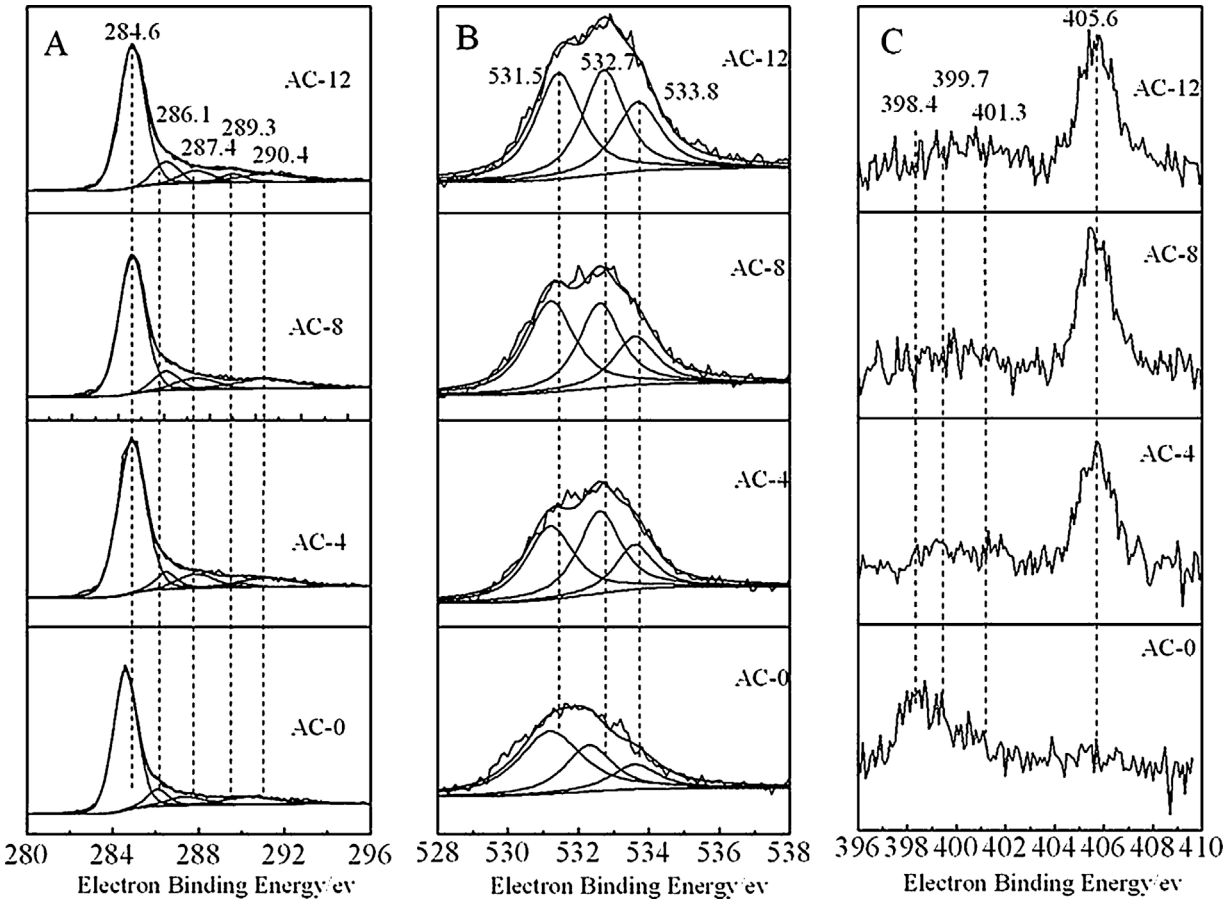

Fig. 1. XPS spectra of C1s (A), O1s (B), and N1s (C) of the AC samples.

Table 3
Carbon, oxygen and nitrogen contents (wt.%) of the AC samples obtained by XPS.

AC Samples	Carbon (wt.%)	Oxygen (wt.%)	Nitrogen (wt.%)
AC-0	91.0	8.0	1.0
AC-4	88.4	10.5	1.1
AC-8	87.1	11.8	1.1
AC-12	84.2	14.7	1.1

of oxygen distinctly increases with the increase of the treatment concentration, and reach the highest (14.7%) when the treatment concentration of HNO_3 is 12 M. But the content of nitrogen almost does not change. This result indicates that HNO_3 treatment concentration mainly influences the amount of surface oxygenated groups. Fu et al. [49] also found that HNO_3 treatment did not change N content too much but can create more surface oxygenated groups.

3.3. XRD and TEM analysis of Cu/AC catalysts

Fig. 2 shows the XRD patterns of the Cu/AC catalysts treated with different concentration of HNO_3. The peaks at 36.5°, 42.2°, 61.3°, and 73.3° are related to the lattice planes of (1 1 1), (2 0 0), (2 2 0), and (3 1 1), respectively in Cu_2O. The peaks at 43.3° and 50.5° are corresponding to the lattice planes of (1 1 1) and (2 0 0) of Cu, while the peaks at 35.5° and 38.5° are attributed to the lattice planes of (1 1 1) and (2 0 0) of CuO. As shown in Fig. 2, when copper supported on the original AC, apart from characteristic peaks of Cu_2O, two obvious characteristic peaks of CuO and a weak characteristic peak of Cu are also detected in XRD patterns. However, after the acid treatment, characteristic peaks of CuO disappear with the enhanced intensity of characteristic peaks of Cu and Cu_2O. It suggests that acid treatment concentration greatly influences the valence of copper species.

The Cu_2O crystallite size is calculated by the Scherrer equation and the results are also listed in Table 4. As the concentration of HNO_3 is below 4 M, the crystallite size of Cu_2O reduces with the increased treatment concentration. Among all the Cu/AC catalysts, Cu/AC-4 attains the smallest crystallite size (11 nm). This result is due to that lower treatment concentrations can generate more surface oxygenated groups on AC that enhance the hydrophilicity of the AC allowing easier access of solutions during the impregnation process and provide additional nucleation sites [40,49], which is

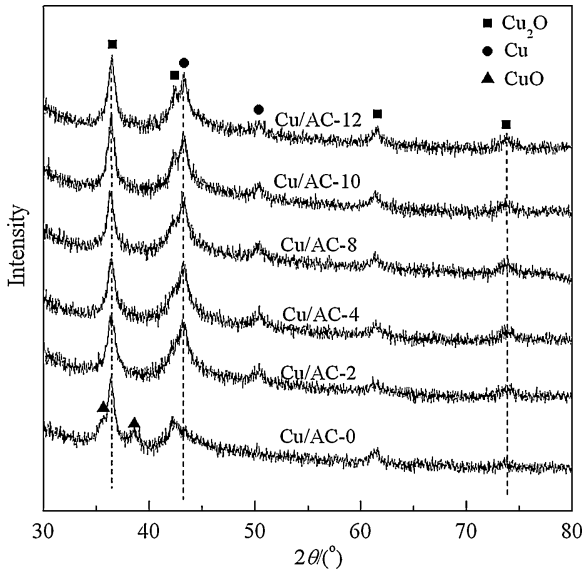

Fig. 2. XRD patterns of the Cu/AC catalysts.

conducive to the dispersion of Cu species of Cu/AC catalysts. However, as shown in Table 4, the crystallite size of Cu_2O increases from 11 nm to 15 nm as the concentration of HNO_3 is raised from 4 M to 12 M, which indicates that higher treatment concentrations are detrimental for the dispersion of Cu species.

The TEM images of Cu/AC catalysts shown in Fig. 3 indicate that the Cu species are distributed uniformly over the surface of AC. The particles size of copper species calculated by nano measure is also listed in Table 4. As shown in Fig. 3, when the HNO_3 concentration is below 4 M, the increase of treatment concentration results in the formation of more dispersed Cu species over AC, confirmed by the decreased average particle size from 32 nm to 12 nm shown in Fig. 3(a)–(c). However, when the HNO_3 concentration is raised from 4 M to 12 M, the particle size of Cu species grows gradually from 12 nm to 25 nm, as shown in Fig. 3(d)–(f). The trend is similar with the XRD Characterization of Cu/AC catalysts. It is worth noting that particle size calculated by TEM is a little bigger than the values calculated by the Scherrer equation. This might be caused by imaging techniques such as TEM which often give the size of the particle, while XRD disclose the size of the crystalline [34]. The dispersion of copper species as well as surface areas of Cu^0 and Cu^+ species was determined by N_2O chemisorption and irreversible CO adsorption (Table 4). It is found that copper dispersion (8.9%), Cu^0 surface area ($2.4\ m^2\ g^{-1}$) and Cu^+ surface area ($2.7\ m^2\ g^{-1}$) obtain the highest on Cu/AC-4. However, further increasing the concentrations of HNO_3 resulted in a gradual decline in both copper dispersion and active copper species surface area.

The concentration of surface oxygenated groups affect the maintenance of the metal dispersion during the precursor decomposition and reduction stage [34,50], and the acidic CO_2-yielding groups (e.g., carboxyl) are thought to be effective catalyst dispersing sites, while the less acidic CO-yielding groups (e.g., carbonyl) are considered to be effective for dispersion maintenance [34]. Coloma and Dandekar et al. [34,51] found that the decreased metal dispersion was due to that the unstable carboxylic groups and carbonyl groups that act as anchoring centers during the impregnation step are decomposed during the high-temperature treatment, which favors the surface mobility of the metal species and leads to a low dispersion. According to previous reports [37,40,52], the carboxylic acids, ketones and aldehydes groups decompose partly at 350 °C which is employed in our experiment. Instead, lactonic and phenolic groups can be effectively maintained owing to their decompose temperature is in the range of 600–800 °C [53,54], which served as the dispersion maintenance site. Boehm's titration results have shown that carboxyl groups, lactonic groups and phenolic groups are the main acidic groups on AC surface. Given the different thermal stability of these groups, the influence of these groups on the copper species dispersion can be divided into two categories: mobility effect and maintenance effect, and the two factors determined the final dispersion of copper species. As the concentration of HNO_3 is above 4 M, the decreased dispersion may be due to that higher treatment concentration of HNO_3 could produce more unstable carboxylic groups, and the decompositions of these groups cause more Cu species mobility and formation of bigger particles during thermal treatment at 350 °C [37].

3.4. XPS and TPR analysis of Cu/AC catalysts

XPS analysis is carried out to elucidate surface Cu components of Cu/AC catalysts. All catalysts $Cu2p_{3/2}$ XPS spectra and their Gaussian fitting figures are displayed in Fig. 4A. In general, $Cu2p_{3/2}$ spectra can be fitted into two peaks corresponding to Cu^{2+} and ($Cu^+ + Cu^0$) for each sample. All the catalysts have two kinds of surface state ($Cu^+ + Cu^0$) and Cu^{2+}; the ratio of the area of the peaks denotes the relative amount of ($Cu^+ + Cu^0$) to Cu^{2+} on the surface. The binding energy in the range of 934.2–934.5 eV can be

Table 4
Copper particle size and surface area analysis of catalysts.

Catalysts	d_{Cu2O} (nm)[a]	d_{Cu} (nm)[b]	d_{Cu} (nm)[c]	Cu dispersion (%)[c]	S_{Cu0} (m^2/g)[c]	S_{Cu+} (m^2/g)[d]
Cu/AC-0	15	32	14.3	5.0	1.2	0.8
Cu/AC-2	13	17	9.7	7.4	1.9	1.9
Cu/AC-4	11	12	8.0	8.9	2.4	2.7
Cu/AC-8	13	14	8.8	8.2	2.2	2.6
Cu/AC-10	14	20	11.3	6.3	1.5	2.0
Cu/AC-12	15	25	13.0	5.5	1.3	1.8
Cu/AC-0 used	–	–	19.3	3.7	0.4	0.6
Cu/AC-4 used	–	21	11.8	6.1	0.9	1.2
Cu/AC-12 used	–	–	25.6	2.9	0.2	0.4

[a] Average diameter of particle size calculated from the XRD diffraction peaks at 2θ of 36.5° for Cu_2O (111) based on the Scherrer equation.
[b] Average particle size determined by TEM.
[c] Determined by N_2O chemisorption.
[d] Determined by CO adsorption.

attributed to Cu^{2+} [55,56], and another binding energy in the range of 932.4–932.5 eV can be assigned to ($Cu^+ + Cu^0$) [57]. The binding energy for Cu^+ and Cu^0 is almost the same, and their difference depends only on the XAES spectra [58]. In the Cu LMM XAES spectra of catalysts (Fig. 4B), asymmetry and broad peaks are observed and deconvoluted into two symmetrical peaks centered at 915.4 and 917.2 eV, corresponding to Cu^0 and Cu^+ species, respectively [58]. The surface Cu species content of Cu/AC catalysts are listed in Table S1.

Temperature-programmed reduction (TPR) is a powerful tool to study the reduction behavior of active phase and metal species in different state. As shown in Fig. 5, all the samples exhibit four partly overlapping peaks. Previous reports [59,60] have shown that the possible sequential reduction of copper is $Cu^{2+} \rightarrow Cu^+ \rightarrow Cu^0$ during

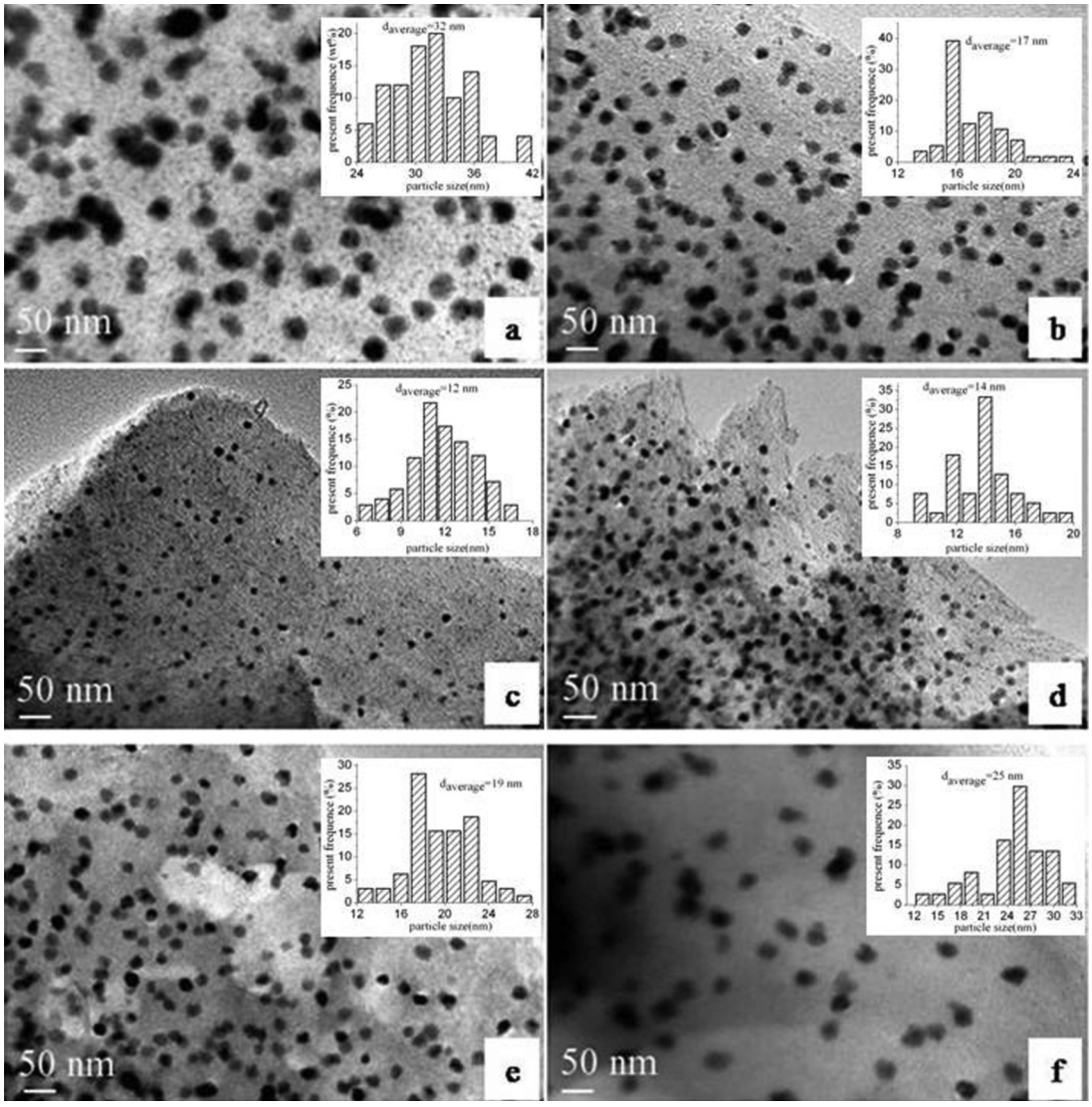

Fig. 3. Representative TEM images of the Cu/AC catalysts. (a) Cu/AC-0, (b) Cu/AC-2, (c) Cu/AC-4, (d) Cu/AC-8, (e) Cu/AC-10, (f) Cu/AC-12.

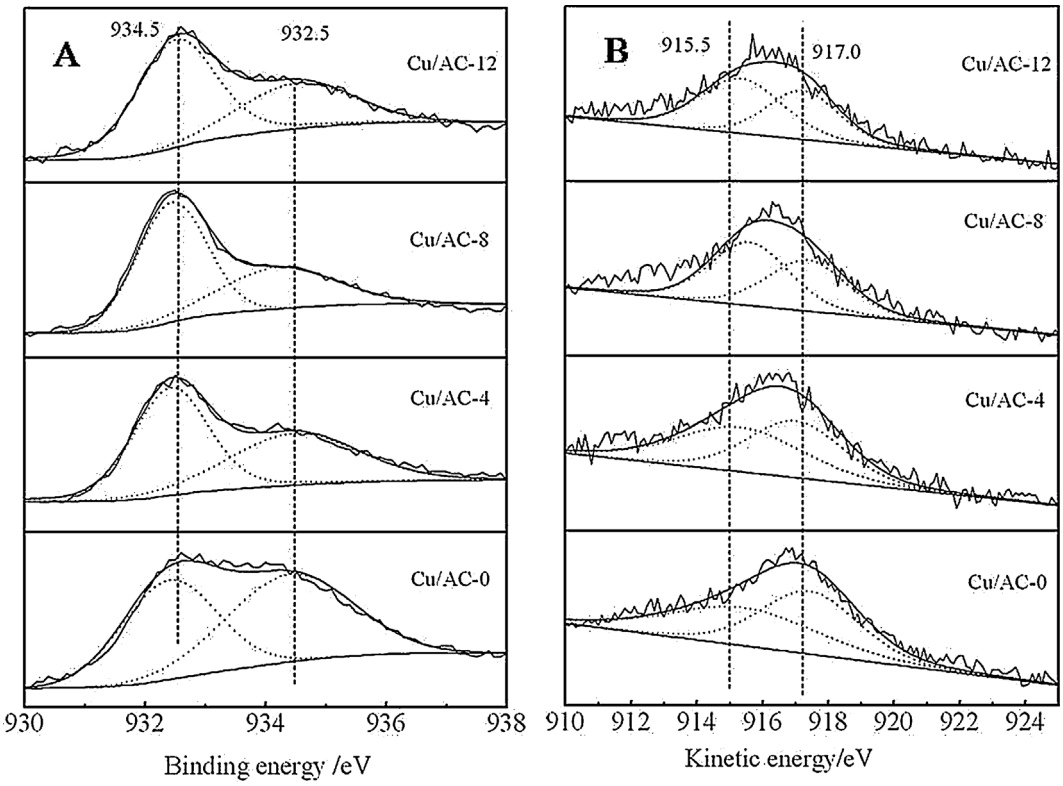

Fig. 4. (A) $Cu2p_{3/2}$ XPS, and (B) Cu LMM Auger spectra of the Cu/AC catalysts.

H_2-TPR profile. The first two peaks around 170–267 °C in the TPR profiles can be attributed to the reduction of highly dispersed and bulk CuO, individually. The third peak around 316–386 °C can be assigned to the reduction of Cu_2O. Besides, the fourth peak above 550 °C can be assigned to the gasification of the carbon support [61].

According to Fig. 5, acid treatment also results in the shift of peak position. The peak positions of CuO shift toward to lower temperature after acid treatment, which indicates that acid treatments enhance the reducibility of CuO over AC. The peaks position of Cu_2O firstly shifts toward to higher temperature with the increase of nitric acid concentration and reaches the maximum when the acid concentration is 4 M. Generally speaking, the degree of interaction with the metal phase and the support varies with the metal particles size, larger metal particles are reduced more easily than smaller ones [62]. This indicates that suitable treatment concentration can increase the interaction between the support and the copper species that resulted in the formation of smaller particles. But as the concentration is above 4 M, the position of that shifts toward to the lower temperature that is due to the grown particles size as shown in Fig. 3(d)–(f). This result is in agreement with the XRD and TEM analysis of Cu/AC catalysts.

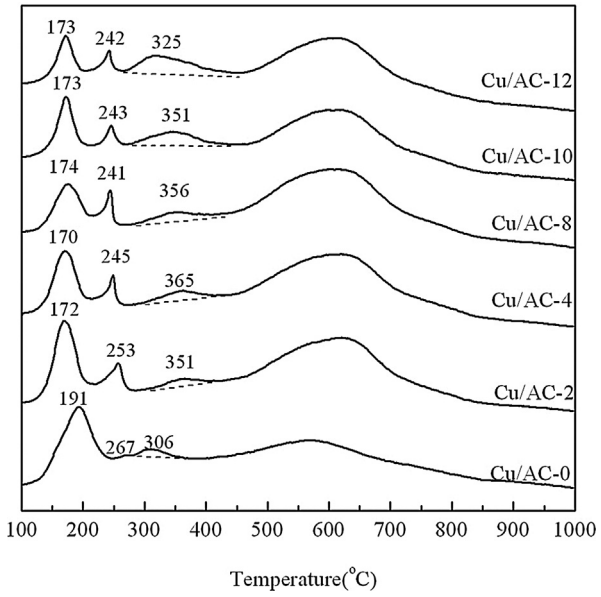

Fig. 5. TPR profiles of the Cu/AC catalysts.

The bulk Cu species content of Cu/AC catalysts based on AAS and H_2-TPR analysis are listed in Table S2. Both the Table S1 nad S2 have shown that the content of Cu^{2+} species gradually decrease with the increase of HNO_3 concentration. Instead, the opposite tendency is observed for the content of Cu^+ and Cu^0 species. Previous study has demonstrated that AC plays both a reducing agent and support role in the formation of Cu–Cu_2O–CuO/AC heterostructure composites [63]. Wang et al. [64,65] found that the more the surface oxygenated groups of AC, the lower the reduction temperature of Cu^{2+} is. Therefore, the phenomenon is presumed to be induced by the increased surface oxygenated groups that may lead to more Cu^{2+} be reduced to Cu^+ or Cu^0. The relationship between the total acidity and the bulk copper valence distributions is shown in Fig. 6, which evidently demonstrates that the amount of surface oxygenated groups greatly affect the valence distributions of copper species.

Moreover, Table 5 has displayed the ratio of Cu^+/Cu^0 for Cu/AC catalysts determined by different methods. It is interesting to find that both the surface and bulk ratio of Cu^+/Cu^0 increase with the increased surface oxygenated groups. The reason may be that there is a competitive mechanism between reduction of Cu^{2+} to Cu^+ and Cu^{2+} to Cu^0 of which the former is preferred. It worth noting that the ratio of Cu^+/Cu^0 (0.9–1.3) on surface is very closely to that in

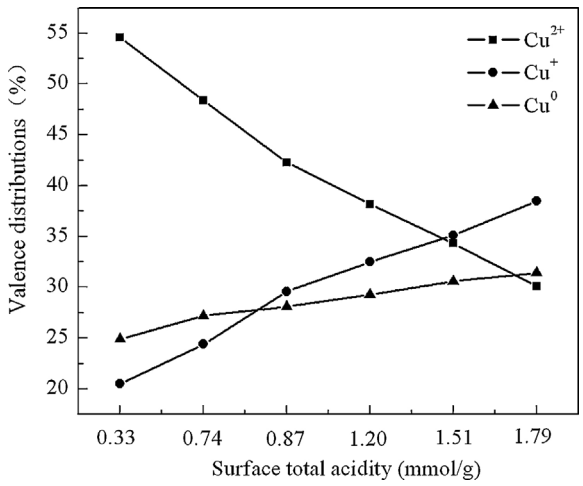

Fig. 6. Influence of surface total acidity on the bulk copper valence distributions of Cu/AC catalysts.

Table 5
Ratio of Cu^+/ Cu^0 for Cu/AC catalysts determined by different methods.

Catalyst samples	Surface (Cu^+/Cu^{0a})	Bulk (Cu^+/Cu^{0b})	(Cu^+/Cu^{0c})
Cu/AC-0	0.9	0.8	0.7
Cu/AC-2	–	0.9	1.0
Cu/AC-4	1.0	1.0	1.1
Cu/AC-8	1.2	1.1	1.2
Cu/AC-10	–	1.1	1.3
Cu/AC-12	1.3	1.2	1.4

[a] Determined from XPS analysis.
[b] Determined from atomic absorption spectrometry (AAS) and H_2-TPR analysis.
[c] Determined from N_2O chemisorptions and CO adsorption.

bulk (0.8–1.2). The similar trend is also observed for the ratio of Cu^+/Cu^0 determined by chemisorption of CO and N_2O.

3.5. Catalytic performance

The catalytic performance of different Cu/AC catalysts for oxidative carbonylation of methanol to DMC are tested in a fixed-bed reactor at the following conditions: 120 °C, n(MeOH):n(CO):n(O_2) = 33:61:6, SV = 2478 h^{-1}, and m_{cat} = 0.8 g. Fig. 7 shows a plot of the DMC synthesis results in terms of space-time yield of DMC (STY_{DMC}) as a function of time on stream. The STY_{DMC} on all the catalysts increase with time, before steadying off within 30 min, after which there is a slowly drop in activity with time. Table 6 shows the average conversion of methanol (C_{MEOH}), selectivity of DMC (S_{DMC}) and STY_{DMC} within 10 h for

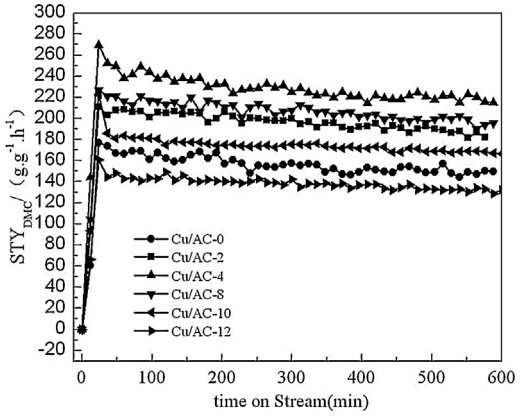

Fig. 7. Variation of STY_{DMC} with time on stream on different Cu/AC catalysts.

the different Cu/AC catalysts. The C_{MEOH} and STY_{DMC} are 6.0% and 157 mg g^{-1} h^{-1} for Cu/AC-0, respectively. After acid treatment of AC, both of these parameters vary with the treatment concentration. When the concentration is below 4 M, the C_{MEOH} and STY_{DMC} have improved with the increase of treatment concentration, and these parameters have attained the highest as the treatment concentration is 4 M. The C_{MEOH} and STY_{DMC} for Cu/AC-4 are 9.2% and 229 mg g^{-1} h^{-1}, respectively. However, when the treatment concentration is above 4 M, these parameters have reduced with the increase of treatment concentration. When the treatment concentration is 12 M, the C_{MEOH} and STY_{DMC} have decreased to 5.7% and 137 mg g^{-1} h^{-1} for Cu/AC-12, respectively.

The treated Cu/AC catalysts by suitable concentration of HNO_3 exhibit the enhanced STY_{DMC} compared to the original Cu/AC catalyst. Characterization results have shown that the amount of surface oxygenated groups greatly increase with the increased acid treatment concentration, while no significant surface area and textural structure changes could be observed in the pore structures when the acid concentration is changed. Thus, we assume that the structures of samples are not the main factors affecting the STY_{DMC}. The treated AC with a suitable amount of surface oxygenated groups have significantly improved dispersion of copper species, whereas a significant decline in copper species dispersion is observed with further increasing the amount of surface oxygenated groups. Among all the catalysts, the Cu/AC-4 catalyst display the highest copper dispersion and the optimized catalytic performance, which implies that high copper dispersion is important to the process of methanol oxidative carbonylation to DMC.

Besides, the increased surface oxygenated groups promote the reduction of Cu^{2+} resulting in that more Cu^+ and Cu^0 species are formed on AC and improve the ratio of Cu^+/Cu^0 as listed in Table 5. However, in our experiment, it is worth noting that the copper dispersion of Cu/AC-12 as well as the surface areas of Cu^+ and Cu^0 species are higher than Cu/AC-0, but its catalytic activity is lower than Cu/AC-0. Li and Wang et al. [24,32] have investigated the effect of copper valence on the methanol oxidative carbonylation to DMC by thermal decomposition of copper precursor under different temperature, and hold that Cu^+ and Cu^0 species were the best active centers, respectively. It is very acknowledged that the copper dispersion varied with the thermal treatment temperature [31]. However, in their study, copper dispersion was not taken into consideration [24,32]. So it is very difficult to determine which copper species is the best active center. According to the literature [66,67], the proposed mechanism of DMC formation by oxidative carbonylation of methanol can be concluded as follows. Firstly, CH_3OH is oxidized to produce the methoxide (MO) species. Then, adsorption and insertion of carbon monoxide into the MO species lead to the formation of monomethyl carbonate species (MMC) as intermediate. Last, the MMC species react with methanol to form DMC. Cu^0 species on AC can effectively adsorb oxygen molecule and CH_3OH, and the adsorbed CH_3OH is converted rapidly to the MO species [18,68]. Instead, Cu^+ in the Y zeolites has been demonstrated to improve the adsorption energy of co-adsorbed CO in co-adsorbed CO/CH_3O system, stabilizes the transition state for the reaction of CO insertion to produces monomethyl carbonate (MMC) species [17,65,69]. Therefore, the possible synthesis process of DMC over Cu/AC catalysts by oxidative carbonylation of methanol is illustrated in Fig. 8. However, it is worth noting that the STY_{DMC} for per S($Cu^+ + Cu^0$) list in Table 6 is in the range of 44–52 mg h^{-1} m^{-2} for the acid treated Cu/AC catalysts, which suggest that the ratio of Cu^+/Cu^0 scarcely affect catalytic performance. Moreover, these value for the acid treated Cu/AC catalysts is less than that (78 mg h^{-1} m^{-2}) of the original Cu/AC catalyst. Recently, some researchers found that AC is not only used as a support for metal dispersion, the amount or kind of surface oxygenated groups itself also plays an important role on the certain catalytic reaction

Table 6
DMC synthesis results for the different Cu/AC catalysts

Catalyst samples	STY_{DMC}/mg g^{-1} h^{-1}	S_{DMC}/%	C_{MEOH}/%	[a]STY_{DMC}/mg h^{-1} m^{-2}
Cu/AC-0	156	62.1	6.0	78
Cu/AC-2	196	56.6	8.2	52
Cu/AC-4	229	59.3	9.2	45
Cu/AC-8	213	57.5	8.8	44
Cu/AC-10	174	59.6	7.0	50
Cu/AC-12	137	56.7	5.7	44

[a] Divided the STY_{DMC} by the specific area ($Cu^+ + Cu^0$).

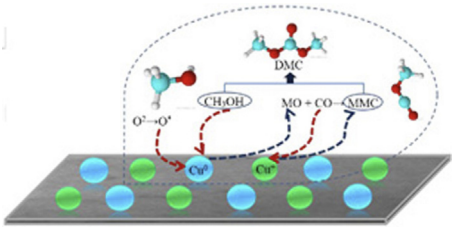

Fig. 8. Possible synthesis process of DMC over Cu/AC catalysts.

[36,37,70]. Therefore, this phenomenon may be induced by the AC surface oxygenated groups itself.

The long-term stability and activity of catalysts are vital for oxidative carbonylation of methanol to dimethyl carbonate from both academic and industrial viewpoints. A comparison of catalytic

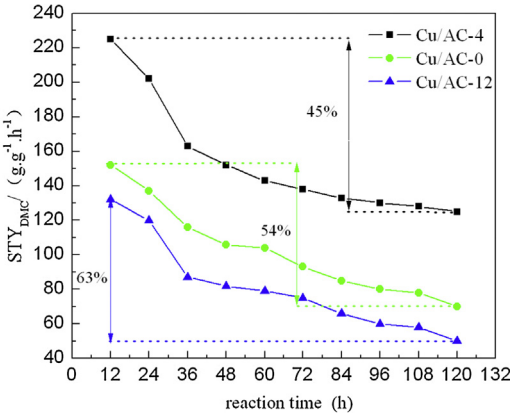

Fig. 9. The long-term catalytic performance of Cu/AC catalysts.

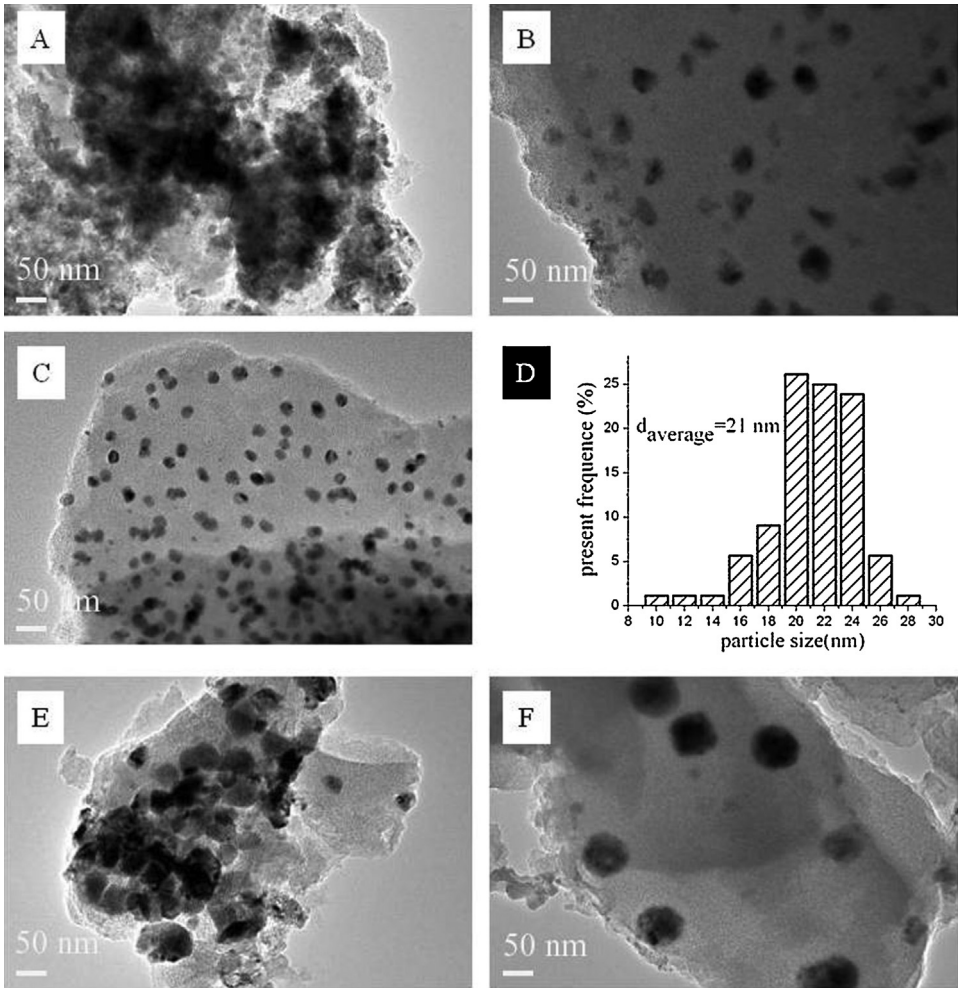

Fig. 10. Representative TEM images of the used Cu/AC catalysts. (A)(B) Cu/AC-0, (C)(D)Cu/AC-4, (E)(F)Cu/AC-12.

activity as a function of reaction time for Cu/AC-0, Cu/AC-4, Cu/AC-12 catalysts is displayed in Fig. 9. All catalysts show deactivation to some extent, but the deactivation degree is very different after evaluated for 120 h. Compared with the initial catalytic activity, the deactivation degree for Cu/AC-0, Cu/AC-4, Cu/AC-12 catalysts are 54%, 45%, and 63%, respectively. In general, the deactivation of supported copper catalysts is attributed to the agglomeration of copper particles, decline in copper dispersion, and change of copper's chemical state [71]. Fig. 10 shows the TEM images for the Cu/AC-0, Cu/AC-4, Cu/AC-12 catalyst after use. Obvious agglomeration of copper species is observed for the used Cu/AC-0 and Cu/AC-12 catalysts, as shown in Fig. 10(A) and (E). As revealed by Fig. 10(B), bigger particles about 42–60 nm are formed on the used Cu/AC-0 compared with 32 nm of the fresh catalyst. Especially for the used Cu/AC-12 catalyst, there are some particles as big as 74–91 nm formed after use (Fig. 10F). However, for the Cu/AC-4 catalyst, the particle size of copper species increases only from 11 to 21 nm and no agglomeration is observed after use. As shown in Table 4, the average particle size determined by N_2O chemisorptions also shows the similar trend with with the TEM results. The long-term catalytic evaluation clearly confirmed that the stability of Cu/AC-4 is significantly higher than that of Cu/AC-0 and Cu/AC-12 catalysts under identified conditions. These experimental results strongly support the viewpoint that the copper agglomeration is the essential reasons for the catalyst deactivation for oxidative carbonylation of methanol.

4. Conclusions

When the coconut shell activated carbon (AC) is treated by nitric acid, no significant change is observed for the texture property of AC, but the surface oxygenated groups are formed and increase gradually with increasing treatment acid concentration. As the concentration of treatment aqueous HNO_3 is below 4 M, the increased surface oxygenated groups are favorable for the copper dispersion. But as the HNO_3 concentration is above 4 M, more unstable carboxylic are produced, and the decomposition of these groups cause the loaded Cu species more mobile and aggregative to form relatively big copper particles during thermal treatment of catalysts at 350 °C. Furthermore, the increased surface oxygenated groups promote the reduction of Cu^{2+} to Cu^+ or Cu^0 as catalytic active centers and the ratio of Cu^+/Cu^0 increases with the increase of the surface oxygenated groups of AC. When Cu supported on AC treated by 4 M HNO_3 aqueous, the catalyst shows the optimal catalytic activity and stability for oxidative carbonylation of methanol to dimethyl carbonate, which might be ascribed to the highest dispersion of Cu^+ and Cu^0 species. However, the STY_{DMC} of per $S(Cu^+ + Cu^0)$ for the acid treated Cu/AC catalysts is very similar and less than that of the original Cu/AC catalyst, which might be induced by the AC surface oxygenated groups itself but not the ratio of Cu^+/Cu^0.

Acknowledgements

The authors are grateful for the financial support from the National Natural Science Foundation of China (21276169) and the National Basic Research Program of China (973 program, 2012CB723105).

Appendix A. Supplementary data

Supplementary data associated with this article can be found, in the online version, at http://dx.doi.org/10.1016/j.apcatb.2015.05.001

References

[1] J. Gong, H. Yue, Y. Zhao, S. Zhao, L. Zhao, J. Lv, S. Wang, X. Ma, J. Am. Chem. Soc. 134 (2012) 13922–13925.
[2] G. Prieto, J.D. Meeldijk, K.P. de Jong, P.E. de Jongh, J. Catal. 303 (2013) 31–40.
[3] S. Zhao, H. Yue, Y. Zhao, B. Wang, Y. Geng, J. Lv, S. Wang, J. Gong, X. Ma, J. Catal. 297 (2013) 142–150.
[4] S. Zhu, X. Gao, Y. Zhu, Y. Zhu, H. Zheng, Y. Li, J. Catal. 303 (2013) 70–79.
[5] E.S. Vasiliadou, T.M. Eggenhuisen, P. Munnik, P.E. de Jongh, K.P. de Jong, A.A. Lemonidou, Appl. Catal. B 145 (2014) 108–119.
[6] X. Gao, S. Liu, Y. Zhang, Z. Luo, K. Cen, J. Hazard. Mater. 188 (2011) 58–66.
[7] D. Gamarra, A.L. Cámara, M. Monte, S.B. Rasmussen, L.E. Chinchilla, A.B. Hungría, G. Munuera, N. Gyorffy, Z. Schay, V.C. Corberán, J.C. Conesa, A. Martínez-Arias, Appl. Catal. B 130–131 (2013) 224–238.
[8] X. Yao, L. Zhang, L. Li, L. Liu, Y. Cao, X. Dong, F. Gao, Y. Deng, C. Tang, Z. Chen, L. Dong, Y. Chen, Appl. Catal. B 150–151 (2014) 315–329.
[9] N. Barrabés, J. Just, A. Dafinov, F. Medina, J.L.G. Fierro, J.E. Sueiras, P. Salagre, Y. Cesteros, Appl. Catal. B 62 (2006) 77–85.
[10] T.T.H. Dang, M. Bartoszek, M. Schneider, D.-L. Hoang, U. Bentrup, A. Martin, Appl. Catal. B 121–122 (2012) 115–122.
[11] S. Huang, P. Chen, B. Yan, S. Wang, Y. Shen, X. Ma, Ind. Eng. Chem. Res. 52 (2013) 6349–6356.
[12] J.D.A. Bellido, E.M. Assaf, Fuel 88 (2009) 1673–1679.
[13] M. Richter, M.J.G. Fait, R. Eckelt, E. Schreier, M. Schneider, M.M. Pohl, R. Fricke, Appl. Catal. B 73 (2007) 269–281.
[14] Y. Zhu, Y. Zhu, G. Ding, S. Zhu, H. Zheng, Y. Li, Appl. Catal. A 468 (2013) 296–304.
[15] G. Prieto, M. Shakeri, K.P. de Jong, P.E. de Jongh, ACS Nano 8 (2014) 2522–2531.
[16] G. Prieto, K.P. de Jong, P.E. de Jongh, Catal. Today 215 (2013) 142–151.
[17] H. Zheng, J. Qi, R. Zhang, Z. Li, B. Wang, X. Ma, Fuel Process. Technol. 128 (2014) 310–318.
[18] J. Ren, W. Wang, D. Wang, Z. Zuo, J. Lin, Z. Li, Appl. Catal. A 472 (2014) 47–52.
[19] Q. Li, H.S. Yang, Z.X. Ma, X.B. Zhang, Catal. Commun. 17 (2012) 8–12.
[20] Y. Xue, G. Lu, Y. Guo, Y. Guo, Y. Wang, Z. Zhang, Appl. Catal. B 79 (2008) 262–269.
[21] Z. Li, C.M. Wen, H.Y. Zheng, K.C. Xie, Chem. J. Chin. Univ. 31 (2010) 145–152.
[22] A.T. Bell, Science 299 (2003) 1688–1691.
[23] K.-H. Chuang, C.-Y. Lu, M.-Y. Wey, Y.-N. Huang, Appl. Catal. A 397 (2011) 234–240.
[24] R.Y. Wang, Z. Li, H.Y. Zheng, K.C. Xie, Chin. J. Catal. 31 (2010) 851–856.
[25] C.Y. Lu, M.Y. Wey, Y.H. Fu, Appl. Catal. A 344 (2008) 36–44.
[26] A.E. Aksoylu, M. Madalena, A. Freitas, M.F.R. Pereira, J.L. Figueiredo, Carbon 39 (2001) 175–185.
[27] X. Zheng, S. Zhang, J. Xu, K. Wei, Carbon 40 (2002) 2597–2603.
[28] Z.H. Zhu, L.R. Radovic, G.Q. Lu, Carbon 38 (2000) 451–464.
[29] J.Y. Rau, H.H. Tseng, B.C. Chiang, M.Y. Wey, M.D. Lin, Fuel 89 (2010) 732–742.
[30] K.-H. Chuang, Z.-S. Liu, M.-Y. Wey, Mater. Sci. Eng. B 175 (2010) 100–107.
[31] Z. Zhu, Z. Liu, S. Liu, H. Niu, T. Hu, T. Liu, Y. Xie, Appl. Catal. B 26 (2000) 25–35.
[32] Z. Li, C.M. Wen, R.Y. Wang, H.Y. Zheng, K.C. Xie, Chem. J. Chin. Univ. 30 (2009) 2024–2031.
[33] L.-Y. Hsu, H. Teng, Appl. Catal. B 42 (2003) 69–76.
[34] A. Dandekar, R.T.K. Baker, M.A. Vannice, J. Catal. 183 (1999) 131–154.
[35] P. Munnik, M. Wolters, A. Gabrielsson, S.D. Pollington, G. Headdock, J.H. Bitter, P.E. de Jongh, K.P. de Jong, J. Phys. Chem. C 115 (2011) 14698–14706.
[36] J. Xu, J. Zhao, J. Xu, T. Zhang, X. Li, X. Di, J. Ni, J. Wang, J. Cen, Ind. Eng. Chem. Res. 53 (2014) 14272–14281.
[37] E.G. Rodrigues, M.F.R. Pereira, X. Chen, J.J. Delgado, J.J.M. Órfão, J. Catal. 281 (2011) 119–127.
[38] C. Alegre, M.E. Galvez, E. Baquedano, R. Moliner, E. Pastor, M.J. Lazaro, J. Phys. Chem. C 117 (2013) 13045–13058.
[39] P. Priyanka, V. Subbaramaiah, V.C. Srivastava, I.D. Mall, Sep. Purif. Technol. 125 (2014) 284–290.
[40] J. Li, L. Ma, X. Li, C. Lu, H. Liu, Ind. Eng. Chem. Res. 44 (2005) 5478–5482.
[41] S. Wang, Z.H. Zhu, Dyes Pigm. 75 (2007) 306–314.
[42] H.-H. Tseng, M.-Y. Wey, Chemosphere 62 (2006) 756–766.
[43] Z.-H. Sheng, L. Shao, J.-J. Chen, W.-J. Bao, F.-B. Wang, X.-H. Xia, ACS Nano 5 (2011) 4350–4358.
[44] B. Xiong, Y. Zhou, Y. Zhao, J. Wang, X. Chen, R. O'Hayre, Z. Shao, Carbon 52 (2013) 181–192.
[45] W. Song, Y. Li, X. Guo, J. Li, X. Huang, W. Shen, J. Mol. Catal. A 328 (2010) 53–59.
[46] T. Horikawa, N. Sakao, T. Sekida, J.i. Hayashi, D.D. Do, M. Katoh, Carbon 50 (2012) 1833–1842.
[47] P.H. Matter, E. Wang, U.S. Ozkan, J. Catal. 243 (2006) 395–403.
[48] V.Z. Radkevich, T.L. Senko, K. Wilson, L.M. Grishenko, A.N. Zaderko, V.Y. Diyuk, Appl. Catal. A 335 (2008) 241–251.
[49] T. Fu, R. Liu, J. Lv, Z. Li, Fuel Process. Technol. 122 (2014) 49–57.
[50] S. Dong Jin, P. Tae-Jin, I. Son-Ki, Carbon 31 (1993) 427–435.
[51] F. Coloma, A. Sepúlveda-Escribano, F. Rodríguez-Reinoso, Appl. Catal. A 123 (1995) L1–L5.
[52] G.S. Szymański, Z. Karpiński, S. Biniak, A. Świątkowski, Carbon 40 (2002) 2627–2639.
[53] J.L. Figueiredo, M.F.R. Pereira, M.M.A. Freitas, J.J.M. Órfão, Carbon 37 (1999) 1379–1389.

[54] J.L. Figueiredo, M.F.R. Pereira, M.M.A. Freitas, J.J.M. Órfão, Ind. Eng. Chem. Res. 46 (2006) 4110–4115.
[55] J.P. Espinós, J. Morales, A. Barranco, A. Caballero, J.P. Holgado, A.R. González-Elipe, J. Phys. Chem. B 106 (2002) 6921–6929.
[56] J.J. Teo, Y. Chang, H.C. Zeng, Langmuir 22 (2006) 7369–7377.
[57] W.Z. Wang, G.H. Wang, X.S. Wang, Y.J. Zhan, Y.K. Liu, C.L. Zheng, Adv. Mater. 14 (2002) 67–69.
[58] F. Raimondi, K. Geissler, J. Wambach, A. Wokaun, Appl. Surf. Sci. 189 (2002) 59–71.
[59] A. Hornés, P. Bera, A.L. Cámara, D. Gamarra, G. Munuera, A. Martínez-Arias, J. Catal. 268 (2009) 367–375.
[60] R. Kefirov, A. Penkova, K. Hadjiivanov, S. Dzwigaj, M. Che, Micropor. Mesopor. Mater. 116 (2008) 180–187.
[61] M. Trépanier, A. Tavasoli, A.K. Dalai, N. Abatzoglou, Appl. Catal. A 353 (2009) 193–202.
[62] M. Trépanier, A.K. Dalai, N. Abatzoglou, Appl. Catal. A 374 (2010) 79–86.
[63] H. Ma, Y. Liu, Y. Fu, C. Yu, X. Dong, X. Zhang, X. Zhang, W. Xue, Aust. J. Chem. 67 (2014) 749–756.
[64] L. Wang, Y. Feng, Y. Zhang, Y. Lou, G. Lu, Y. Guo, Fuel 96 (2012) 440–445.
[65] L. Wang, Y. Zhou, Q. Liu, Y. Guo, G. Lu, Catal. Today 153 (2010) 184–188.
[66] J. Engeldinger, M. Richter, U. Bentrup, Phys. Chem. Chem. Phys. 14 (2012) 2183–2191.
[67] Y. Zhang, A.T. Bell, J. Catal. 255 (2008) 153–161.
[68] H.Y. Zheng, Y. Qin, Z. Li, G.Q. Zhang, F.H. Meng, Chin. J. Inorg. Chem. 30 (2014) 2111–2118.
[69] R. Zhang, J. Li, B. Wang, RSC Adv. 3 (2013) 12287–12298.
[70] M.L. Toebes, F.F. Prinsloo, J.H. Bitter, A.J. van Dillen, K.P. de Jong, J. Catal. 214 (2003) 78–87.
[71] R.G. Wall. Pinole, CA, US 4, 149, 021, 1978.